J Eng Math (2008) 62:315–331
DOI 10.1007/s10665-007-9208-9

Eddy currents in a transverse MRI gradient coil

J. M. B. Kroot · S. J. L. van Eijndhoven · A. A. F. van de Ven

Received: 2 February 2007 / Accepted: 16 November 2007 / Published online: 30 January 2008

Abstract A transverse gradient coil (x- or y-coil) of an MRI-scanner is modeled as a network of curved circular strips placed at the surface of a cylinder. The current in this network is driven by a time-harmonic source current. The low frequency applied allows for an electro-quasi-static approach. The strips are thin and the current is assumed to be uniformly distributed in the thickness direction. For the current distribution in the width direction of the strips, an integral equation is derived. Its logarithmically singular kernel represents inductive effects related to the occurrence of eddy currents. For curved circular strips of width much smaller than the radius of the cylinder one may *locally* replace the curved circular strip by a tangent plane circular strip. This plane geometry preserves the main characteristics of the transverse current distribution through the strips. The current distribution depends strongly on the in-plane curvature of the strips. The Petrov–Galerkin method, using Legendre polynomials, is applied to solve the integral equation and shows fast convergence. Explicit results are presented for two examples: a set of 1 strip and one of 10 strips. The results show that the current distributions are concentrated near the inner edges and that resulting edge-effects, both local and global, are non-symmetric. This behavior is more apparent for higher frequencies and larger in-plane curvatures. Results have been verified by comparison with finite-element results.

Keywords Eddy currents · Edge-effect · Legendre polynomials · MRI-scanner · Transverse gradient coils

1 Introduction

Magnetic Resonance Imaging (MRI) is a revolutionary way of scanning in medical diagnostics, producing images with contrast differences. MRI utilizes gradient coils to induce magnetic-field gradients for the spatial differentiation of the signals emitted from parts of the human body to be diagnosed. A gradient magnetic field is an alternating magnetic field, superimposed on a strong static and substantially uniform magnetic field, which changes linearly with position. For a detailed description of MRI we refer to e.g. [1,2].

The gradient coils of an MRI-scanner consist of copper strips on a cylinder. They are designed such that alternating electric currents through the coils cause the magnetic field to have a uniform gradient in a specific region of interest. High precision of the gradient field is crucial for reliable high-quality images. Thus, research is carried out on the development of eddy currents in the gradient coils, which have a negative effect on the uniformity of the

J. M. B. Kroot · S. J. L. van Eijndhoven · A. A. F. van de Ven (✉)
Eindhoven University of Technology, P.O. Box 513, 5600 MB, Eindhoven, The Netherlands
e-mail: a.a.f.v.d.ven@tue.nl

gradient field. In previous work ([3,4]), networks of plane straight strips and of coaxial rings were considered. It was shown that a longitudinal or z-coil can be modeled by a set of circular loops of strips (rings) around the cylinder. By properly selecting the positions of the loops and the magnitudes of the currents, one can achieve a uniform gradient field of high precision. Different design solutions are presented by, e.g., Romeo and Hoult [5] or Suits and Wilken [6]. In other methods, the values of the currents are fixed and the corresponding positions are computed. This leads to optimization methods, such as the conjugate gradient method by Wong and Jesmanowicz [7] and the simulated annealing method by Crozier and Doddrell [8]. Other basic methods for the design of x- and y-coils are described by Frenkiel et al. [9] or Siebold [10]. A standard example of a coil that creates a magnetic field whose axial component is linearly increasing in the transversal direction is the Golay coil. The Golay coil consists of four sets of symmetrically placed saddle coils. The optimal dimensions are determined using zonal spherical harmonics. For more details on the Golay coil, see [1,Sect. 3.4]. In the practical design of gradient coils, first, for a DC source current the optimal distribution of streamlines, representing one-dimensional wires, is determined and, then, thin strips of copper are placed along these streamlines. The magnetic field induced by the currents in the conductor pattern is computed, assuming that the current density is uniform in the strips. For an optimal distribution of streamlines, often stream functions are used; see [11–14].

The present paper focusses on a mathematical model of the current distribution in the *transverse gradient coils* of the scanner. Since strips of finite width (instead of wires) are used in the manufacture of a gradient coil, eddy currents occur. The eddy currents cause extra dynamic forces on the conductors that result in noise and reduction of lifetime. More importantly, the eddy currents cause perturbations of the expected gradient field, leading to MR pictures with blurring and ghosting. Eddy-current response is greatly affected by the frequencies used, by geometrical features such as curvature, edges, grooves, and by the distances between conductors.

The main objective of this paper is to determine the current distribution within the strips. In contrast to the currently used streamline methods, in which the current in a strip is assumed to be uniformly distributed, we include eddy currents, making the current distribution non-uniform, thus affecting the linearity of the gradient field and consequently the quality of the images.

In previous work, we have determined the eddy currents in sets of plane rectangular strips [3] and parallel coaxial rings [4]. In both papers, an integral equation for the current is derived and the Galerkin method is used to solve the integral equation. Legendre polynomials turned out to be a very appropriate choice of the basis functions, because of fast convergence and the analytical way to overcome the logarithmic singularity in the kernel of the integral equation. The results in both plane rectangular strips and rings show edge-effects in the currents and phase-lag with respect to the source. The main conclusion after comparing the results of [3] and [4] is that the curvature of the rings hardly affects the current distribution, as compared with that of the plane strips, provided the radius of the rings is always much larger than their width.

In this paper, we consider configurations of one or more closed circular loops of strips placed on top of a cylinder. These circular strips form an appropriate geometry to model a transverse gradient coil. In contrast to the rings, these strips have two characteristic curvatures: the (global) curvature of the basic cylinder and the (in-plane) curvature of the circular central line of the strip on the cylinder. Since the radius of the cylinder is always much larger than the width of the strips, the global curvature is not so relevant, but the in-plane curvature will play a dominant role. The strips are conductors and carry a time-harmonic electric current. In this respect, we note that gradient coils are switched on and off rapidly for slice selection and amplitude and phase encoding. A typical switching sequence consists of trapezoidal pulses. These pulses are composed in practice by a limited series of harmonics. Hence, the analysis can assume a superposition of time-harmonic currents as well, and only a few frequencies are needed. In the numerical results we will present, a range of frequencies of the significant Fourier components are used that are practically relevant for MRI applications. The thin strips have an almost uniformly distributed current density in the thickness direction, implying that the thin strip can be modeled as a 2-D surface and the current density (A/m^2) as a surface current (A/m). The current in the strips is in tangential direction (along the central line), but non-uniformly distributed in the transverse (width) direction. For this current distribution, an integral equation with a singular logarithmic kernel is derived. The non-uniformity of the current is not only due to the, dynamic, eddy currents, but also to the, static, $1/r$ effect: the static (or DC) current is inversely proportional to the radial distance r measured

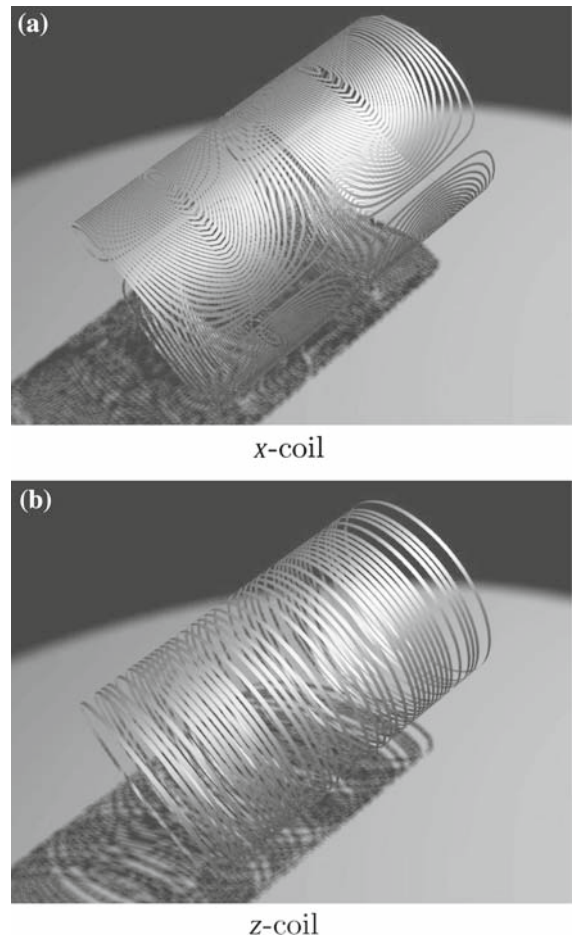

Fig. 1 (**a**) Sketch of the x-coil. The y-coil has an identical shape and is placed in the scanner with a rotation of 90 degrees about the x-coil; (**b**) Sketch of the z-coil

with respect to the center of the circular strip. To account for this $1/r$ effect, the Petrov–Galerkin method is used to solve the integral equation.

We start this paper with the problem formulation and the derivation of the basic integral equation in Sect. 2. In Sect. 3, the solution procedure for this integral equation is presented, while numerical results for two different types of transverse gradient coils are given in Sect. 4. Explicit results are depicted for the transverse current distributions and for the electric resistances of the coils. We show how due to the $1/r$ effect and the eddy currents the current distribution on the strips is shifted towards the inner edges of the strips. This effect is getting stronger as the in-plane curvature of the strip and the frequency of the time-harmonic current increase.

2 Problem formulation

A gradient coil consists of a long strip of copper arranged on a cylinder. Figure 1 shows design configurations of gradient coils. As can be seen from this figure, the strips on a transverse (x- or y-) coil form circles on top of the cylinder, whereas the z-coil consists of a set of parallel circular strips (rings) around the cylinder. The width of a strip is a few centimeters, its thickness a few millimeters, and a common value for the radius of the cylinder is 35 cm. The mutual distance between separate windings of the coil varies from just a few millimeters to several centimeters. As in [3] and [4], the strips are of uniform width; however, not all the strips need to have the same width and mutual distances may be different.

A comparison of the results of [3] and [4] revealed that inductance effects are local; see the second paragraph of [4, Sect. 5]. Induction causes the non-uniformness of the transverse current distribution. This leads us to the following conclusion: the current distribution in transverse direction in a point on a strip of width D is only affected by the currents in a D-vicinity (distances of a few times D) of that point. Mathematically, the basic reason is that the logarithmic part of the kernel of our fundamental integral equation governs the principal behavior of the current. This logarithmic kernel is the same for a straight and a curved strip, and the approximation made by replacing the whole kernel for the curved ring by only its logarithmic part is of $O(D^2/R^2)$, for $D/R \ll 1$. Therefore, replacing the cylindrically curved loop locally by a plane circular loop in the tangent plane on the cylinder in the same point is allowed within the same order of accuracy. As long as we are only interested in the transverse current distribution, this replacement by a plane circular loop is justified. However, it must be emphasized that this is not allowed when we want to calculate the magnetic field induced by the currents in the curved circular loops on top of the cylinder. All this holds irrespective of the in-plane radius of the circular loop; even if this radius becomes of the order of magnitude of a few times D, this approximation is still allowed.

Hence, since in this paper we focus on the transverse current distributions in the strips, we can approximate the strips, locally, by plane circular strips. The configuration of a set of plane circular loops is depicted in Fig. 2. In this plane configuration, we introduce a radial coordinate r, measured from the center of the circle (the notation r should not be confused with the r-coordinate of a set of cylindrical coordinates attached to the cylinder), and a tangential coordinate φ, as shown in Fig. 2.

We consider a set of N distinct plane circular strips of uniform width and thickness. The thickness of all strips is h, which is very small compared to their widths. Therefore, the current distribution through the thickness is fairly uniform (see [4]) and thus the resulting current can be considered as a surface current $\mathbf{j}$ on an infinitely thin strip. The circular strips are lying concentrically in a plane; see Fig. 2. Not all strips are necessarily of the same width and their mutual distances may differ. Because the geometry is rotationally symmetric and the current divergence-free, the current does not depend on φ and has a component in the φ-direction only, so $\mathbf{j} = j(r)\mathbf{e}_\varphi$. The current distribution $j(r)$ is the unknown function we want to calculate here.

The loops occupy a surface $S_\cup$ on the plane. The set of loops is subdivided into L groups, each of which is driven by a separate source current and has a prescribed time-harmonic total current $I_l(t) = \mathfrak{Re}\{I_l \mathrm{e}^{-\mathrm{i}\omega t}\}, l = 1, \ldots, L$, with $I_l \in \mathbb{C}$ a complex constant. The sum of the widths of all loops in group l is denoted by D_l. The number of loops in each group is denoted by N_l. Then, $S_n^{(l)}$ can be defined as the surface of the nth loop within group l, with $n \in \{1, \ldots, N_l\}$ and $S_\cup^{(l)}$ as the surface occupied by the strips in the l th group. Hence,

$$S_\cup^{(l)} = \sum_{n=1}^{N_l} S_n^{(l)}, \quad \text{and} \quad S_\cup = \sum_{l=1}^{L} S_\cup^{(l)} = \sum_{l=1}^{L}\sum_{n=1}^{N_l} S_n^{(l)}, \tag{1}$$

where $\sum$ denotes disjoint union of sets. Note that $S_n^{(l)} \subset S_\cup^{(l)} \subset S_\cup$.

Since the currents do not depend on φ, it is more convenient to introduce a notation for the r-intervals in which the loops are positioned. Instead of $S_\cup$, which represents a surface, we introduce the one-dimensional set $S_\cup^r$ as the collection of all radial intervals of the loops:

$$S_\cup^r = \sum_{n=1}^{N} S_n^r, \quad S_n^r = \{r | r_0^{(n)} < r < r_1^{(n)}\}. \tag{2}$$

The current distribution $j(r)$ satisfies an integral equation that is derived from the Maxwell equations in the same way as in [3] and [4]. Thereby we use the assumption that the low frequency ω of the time-harmonic fields allows an electro-quasi-static approach; see [4, Sect. 2].

To make our formulation dimensionless, let j^c be the characteristic value for the surface current through the strips, and R^c the characteristic length, successively defined by

$$j^c = \frac{\sum_{l=1}^{L} I_l}{\sum_{l=1}^{L} D_l}, \qquad R^c = r_0^{(1)}. \tag{3}$$

Thus, the current is scaled by the average current through all strips and the distances are scaled by the inner radius of the first loop. We can write the complex amplitude of the vector potential $\mathbf{A}$ at position $\mathbf{x}$ in a dimensionless form $\tilde{\mathbf{A}}$, according to

$$\mathbf{A}(\mathbf{x}) = \mu_0 R^c j^c \tilde{\mathbf{A}}(\tilde{\mathbf{x}}), \tag{4}$$

where

$$\tilde{\mathbf{A}}(\tilde{\mathbf{x}}) = \frac{1}{4\pi} \int_{S_\cup} \frac{\tilde{\mathbf{j}}(\tilde{\boldsymbol{\xi}})}{|\tilde{\mathbf{x}} - \tilde{\boldsymbol{\xi}}|} \, \mathrm{d}a(\tilde{\boldsymbol{\xi}}). \tag{5}$$

Here, μ_0 is the magnetic permeability, $\tilde{\mathbf{x}} = \mathbf{x}/R^c$ is the dimensionless position of the observation point, and $\tilde{\mathbf{j}}$ is the dimensionless current, scaled by j^c. This means that $\mathbf{j}(\mathbf{x}, t) = \Re\mathfrak{e}\{j^c \tilde{\mathbf{j}}(\tilde{\mathbf{x}}) \mathrm{e}^{-\mathrm{i}\omega t}\}$. In the sequel, we consider only the spatial parts of the fields; time derivatives are replaced by $-\mathrm{i}\omega$. The tildes are omitted from now on.

On the plane circular strips, we denote the observation point $\mathcal{P}$ and the source point $\mathcal{Q}$ by vectors $\mathbf{p} = \mathbf{p}(r, \varphi)$ and $\mathbf{q} = \mathbf{q}(\rho, \theta)$, which in polar coordinates are given by

$$\mathbf{p} = r\mathbf{e}_r(\varphi), \qquad \mathbf{q} = \rho \mathbf{e}_\rho(\theta) = \rho \cos(\varphi - \theta)\mathbf{e}_r - \rho \sin(\varphi - \theta)\mathbf{e}_\varphi. \tag{6}$$

The distance between the points $\mathcal{P}$ and $\mathcal{Q}$ is

$$|\mathbf{p} - \mathbf{q}| = \sqrt{(r - \rho)^2 + 4r\rho \sin^2\left(\frac{\varphi - \theta}{2}\right)}. \tag{7}$$

Substituting $\mathbf{j}(\boldsymbol{\xi}) = j(\rho)\mathbf{e}_\theta = j(\rho)\sin(\varphi - \theta)\mathbf{e}_r + j(\rho)\cos(\varphi - \theta)\mathbf{e}_\varphi$ in (5), we obtain the components of the vector potential $\mathbf{A} = \mathbf{A}(r)$ according to

$$A_r(r) = \frac{1}{4\pi} \int_{S_\cup} \frac{\sin(\varphi - \theta) j(\rho)}{\sqrt{(r - \rho)^2 + 4r\rho \sin^2(\frac{\varphi - \theta}{2})}} \, \mathrm{d}a(\rho, \theta) = 0, \tag{8}$$

$$A_\varphi(r) = \frac{1}{4\pi} \int_{S_\cup} \frac{\cos(\varphi - \theta) j(\rho)}{\sqrt{(r - \rho)^2 + 4r\rho \sin^2(\frac{\varphi - \theta}{2})}} \, \mathrm{d}a(\rho, \theta), \tag{9}$$

where the surface element $\mathrm{d}a(\rho, \theta) = \rho \, \mathrm{d}\rho \, \mathrm{d}\theta$. The component $A_r = 0$, because the integrand of the integral on the right-hand side is an odd function of $(\varphi - \theta)$.

To arrive at an integral equation for the current, we use the relation between the electric field $\mathbf{E}$ and the vector potential $(\mathbf{E}, \mathbf{e}_\varphi) = E_\varphi = \mathrm{i}\omega A_\varphi$, apply the continuity of the tangential component of the $\mathbf{E}$-field at the surface of the strip and then Ohm's law in the form $j = \sigma h E_\varphi + j^s = \mathrm{i}\omega\sigma h A_\varphi(r) + j^s(r)$, where σ is the electric conductivity (the factor h is added because j is a surface current) and j^s is a source current (see [4, Eq. (6)]). Thus, after dimensionalization, we obtain

$$j(r) - \frac{\mathrm{i}\kappa}{4\pi} \int_{S_\cup} \frac{\cos(\theta) j(\rho)}{\sqrt{(r - \rho)^2 + 4r\rho \sin^2(\frac{\theta}{2})}} \, \mathrm{d}a(\rho, \theta) = j^s(r), \tag{10}$$

where

$$\kappa = h\sigma\mu_0\omega R^c. \tag{11}$$

Since $S_\cup = S^r_\cup \times [-\pi, \pi]$, repeated integration yields

$$\begin{aligned} j(r) - j^s(r) &= \frac{\mathrm{i}\kappa}{2\pi} \int_{\mathcal{S}^r_\cup} \left[\int_{-\pi/2}^{\pi/2} \frac{\cos(2\theta)}{\sqrt{(r + \rho)^2 - 4\cos^2(\theta)}} \, \mathrm{d}\theta \right] \rho j(\rho) \, \mathrm{d}\rho \\ &= \frac{\mathrm{i}\kappa}{2\pi} \int_{\mathcal{S}^r_\cup} \frac{1}{k\sqrt{r\rho}} [(2 - k^2)K(k) - 2E(k)] \rho j(\rho) \, \mathrm{d}\rho. \end{aligned} \tag{12}$$

Here, $K(k)$ and $E(k)$ are the complete elliptic integrals of the first and second kind ([15, Sect. 17]), respectively, and

$$k = \frac{2\sqrt{r\rho}}{r+\rho}. \tag{13}$$

The source current is a time-harmonic current, but its spatial part is independent of the frequency ω, as this spatial part is equal to the DC source current ($\omega = 0$).

3 Solution method

3.1 Construction of a linear set of equations

The Petrov–Galerkin method, used to solve the integral equation (12), is first applied to a single circular strip: $S_{\cup}^{r} = \{r|1 < r < r_1/r_0\}$. The case of more strips is treated in the same way and explained further on.

Let the current distribution j be expanded in a series of basis functions ϕ_m, with corresponding coefficients α_m, according to

$$j = \sum_{m=0}^{\infty} \alpha_m \phi_m. \tag{14}$$

The source current j^s is expanded in the same basis functions ϕ_m, but with coefficients β_m,

$$j^s = \sum_{m=0}^{\infty} \beta_m \phi_m. \tag{15}$$

For an appropriate choice of the basis functions, we are led by the solution for the DC-situation. For $\omega \to 0$ (equivalently, $\kappa \to 0$), the inductive effects disappear and $j \to j^s$. The analytical solution for the static current distribution in one plane circular loop, carrying a total current I, is given by

$$j = \frac{I}{R^c j^c \log(r_1/r_0)} \frac{1}{r} = \frac{D}{r_0 \log(r_1/r_0)} \frac{1}{r}. \tag{16}$$

Consequently, the current is inversely proportional to r (where one should read $\tilde{r} = r/r_0$ for r).

The kernel of the integral equation (12) has a logarithmic singularity in $r = \rho$ (i.e., $k = 1$). Therefore, we approximate j by a series of scaled and shifted Legendre polynomials divided by r, according to

$$\phi_m(r) = \frac{1}{r} P_m\left(\frac{r-c}{d}\right), \tag{17}$$

where

$$c = \frac{r_1 + r_0}{2r_0}, \qquad d = \frac{r_1 - r_0}{2r_0}. \tag{18}$$

As was said before, the spatial behavior of the source current is the same for all frequencies ω, including $\omega = 0$. This yields, with $P_0(r) = 1$,

$$\beta_0 = \frac{I}{R^c j^c \log(r_1/r_0)}, \qquad \beta_m = 0, \qquad m \geq 1. \tag{19}$$

The coefficients $\alpha_m, m \geq 0$, depend on the frequency ω. Only for $\omega = 0$ we know them a priori: $\alpha_0 = \beta_0$, $\alpha_m = 0, m \geq 1$, because for $\omega = 0$ inductive effects are absent. The total current condition for one strip reads

$$\int_{r_0}^{r_1} j(\rho)\, \mathrm{d}\rho = \alpha_0 \log\left(\frac{r_1}{r_0}\right) + d \sum_{m=1}^{M} \alpha_m \int_{-1}^{1} \frac{P_m(r)}{dr + c}\, \mathrm{d}r = \frac{I}{R^c j^c}. \tag{20}$$

We apply a projection method with test functions different from basis functions and use the inner product

$$(f, g) = \int_{S_\cup^r} f(r)g(r)r \, \mathrm{d}r. \tag{21}$$

The basis functions are Legendre polynomials of the first kind divided by r (see (17)) while the test functions are the Legendre polynomials themselves, i.e., $P_m((r-c)/d)$. Their mutual inner products are

$$\int_{r_0}^{r_1} \frac{P_m(\frac{\rho-c}{d})}{\rho} P_n\Big(\frac{\rho-c}{d}\Big)\rho \, \mathrm{d}\rho = \frac{2d}{2m+1}\delta_{mn}. \tag{22}$$

Thus, the source current only yields a non-zero inner product for the zeroth-order test function P_0. This is the main reason to use the Petrov–Galerkin method. It enables us to embed the source current in the family of basis functions such that the total current density is expanded into components that comprise the source current density.

Next, we generalize the method for two or more plane circular loops. Let ψ_l be the characteristic function of group l,

$$\psi_l = \sum_{n=1}^{N_l} \mathbf{1}_{[r_0^{(n)}, r_1^{(n)}]}, \tag{23}$$

where $\mathbf{1}_{[a,b]}$ represents the characteristic function of the interval $[a, b]$. In (23), $r_0^{(n)}$ and $r_1^{(n)}$ are dimensionless, scaled on $R^c = r_0^{(1)}$. Due to disjointness of the intervals S_Ω^l, each two characteristic functions $\psi_{l_1}, \psi_{l_2}, l_1, l_2 \in \{1, 2, \ldots, L\}$ satisfy

$$\Big(\frac{\psi_{l_1}}{r}, \psi_{l_2}\Big) = \frac{D_{l_1}}{R^c}\delta_{l_1 l_2}. \tag{24}$$

The source current j^s is in every loop inversely proportional to r and can therefore be written as

$$j^s = \sum_{l=1}^{L} C_l \frac{\psi_l}{r}, \tag{25}$$

with unknown constants C_l. The integral equation (12) then becomes

$$j(r) - i\kappa \int_{S_\cup^r} \mathcal{K}(r, \rho) j(\rho)\rho \, \mathrm{d}\rho = \sum_{l=1}^{L} C_l \frac{\psi_l(r)}{r}, \quad r \in S_\cup^r, \tag{26}$$

with

$$\mathcal{K}(r, \rho) = \frac{1}{2\pi k\sqrt{r\rho}}[(2-k^2)K(k) - 2E(k)], \qquad k = \frac{2\sqrt{r\rho}}{r+\rho}. \tag{27}$$

Moreover, the total current per group is prescribed, so $j(r)$ must satisfy

$$\int_{S_\cup^r} j(\rho)\psi_l(\rho) \, \mathrm{d}\rho = \Big(\frac{1}{r} j, \psi_l\Big) = \hat{I}_l, \qquad l = 1, \ldots, L, \tag{28}$$

where $\hat{I}_l = I_l/(j^c R^c)$, with j^c according to (3).

We define the operator K on $L_2(S_\cup^r, r \, \mathrm{d}r)$ by

$$(\mathsf{K}f)(r) = \int_{S_\cup^r} f(\rho)\mathcal{K}(r-\rho)\rho \, \mathrm{d}\rho, \tag{29}$$

and then (26) can be written in operator form as

$$(\mathrm{I} - \mathrm{i}\kappa\mathsf{K}) j = \sum_{l=1}^{L} C_l \frac{\psi_l}{r}. \tag{30}$$

We define the projection Π on the linear span of the characteristic functions $r^{-1}\psi_l$, $l \in \{1, \ldots, L\}$, by

$$(\Pi f) = \sum_{l=1}^{L} \frac{(f, \psi_l)}{(\frac{1}{r}\psi_l, \psi_l)} \frac{\psi_l}{r}. \tag{31}$$

The projection Π applied to j yields, by use of (24),

$$\Pi j = \sum_{l=1}^{L} R^c \frac{(j, \psi_l)}{D_l} \frac{\psi_l}{r} = \sum_{l=1}^{L} \alpha_0^{(l)} \frac{\psi_l}{r}, \tag{32}$$

where the coefficients $\alpha_0^{(l)}$ are defined by $\alpha_0^{(l)} = R^c(j, \psi_l)/D_l$, $l = 1, \ldots, L$.

We note that, although $\Pi^2 = \Pi$, Π is not orthogonal, because $\Pi^* \neq \Pi$ as

$$(\Pi^* f) = \sum_{l=1}^{L} \frac{(f, \frac{1}{r}\psi_l)}{(\frac{1}{r}\psi_l, \psi_l)} \psi_l \neq (\Pi f). \tag{33}$$

Moreover, we note that (28) cannot be used here in the same way as in [3,4], where the coefficients of the basis functions ψ_l disappeared in favor of the total currents $\hat{I}_l$. Hence, we cannot directly eliminate the unknown coefficients $\alpha_0^{(l)}$ here.

Next, j is split into two parts according to

$$j = \Pi j + (\mathrm{I} - \Pi) j = \sum_{l=1}^{L} \alpha_0^{(l)} \frac{\psi_l}{r} + j_\perp. \tag{34}$$

Here, $j_\perp = (\mathrm{I} - \Pi) j$ is in the range of Π^*, i.e., $(j_\perp, \psi_l) = 0$, for $l = 1, \ldots, L$. Applying the operator $(\mathrm{I} - \Pi)$ to (30), we obtain

$$j_\perp - \mathrm{i}\kappa(\mathrm{I} - \Pi)\mathsf{K} j = 0, \tag{35}$$

or equivalently,

$$j_\perp - \mathrm{i}\kappa(\mathrm{I} - \Pi)\mathsf{K} j_\perp = \mathrm{i}\kappa \sum_{l=1}^{L} \alpha_0^{(l)} (\mathrm{I} - \Pi)\mathsf{K}\frac{\psi_l}{r}. \tag{36}$$

In this relation for $j_\perp$, the constants C_l have disappeared, but they are replaced by the coefficients $\alpha_0^{(l)}$, which are also unknown a priori. For this, we should use the L known values $\hat{I}_l$, $l = 1, \ldots, L$, for which we need an additional set of L equations. These equations are obtained from the inner products of relation (30) with ψ_l, $l = 1, \ldots, L$.

We approximate $j_\perp$ by a finite series of basis functions $\phi_m \in \mathrm{ran}(I - \Pi)$,

$$j_\perp \doteq \sum_{m=1}^{M} \alpha_m \phi_m. \tag{37}$$

Taking successively the inner product of (30) with ψ_l and (36) with $r\phi_n$, we arrive at

$$\alpha_0^{(l)} \frac{D_l}{R^c} - \mathrm{i}\kappa \sum_{k=1}^{L} \alpha_0^{(k)} \left(\mathsf{K}\frac{\psi_k}{r}, \psi_l\right) - \mathrm{i}\kappa \sum_{m=1}^{M} \alpha_m (\mathsf{K}\phi_m, \psi_l) = \frac{D_l}{R^c} C_l, \qquad l = 1, \ldots, L, \tag{38}$$

$$\sum_{m=1}^{M} \alpha_m (\phi_m, r\phi_n) - \mathrm{i}\kappa \sum_{l=1}^{L} \alpha_0^{(l)} \left(\mathsf{K}\frac{\psi_l}{r}, r\phi_n\right) - \mathrm{i}\kappa \sum_{m=1}^{M} \alpha_m (\mathsf{K}\phi_m, r\phi_n) = 0, \qquad n = 1, 2, \ldots, M. \tag{39}$$

For convenience of notation, we write (38) and (39) in matrix form as

$$(\mathbf{G} - \mathrm{i}\kappa\mathbf{A})\mathbf{a} = \mathbf{c}, \tag{40}$$

where the block matrices $\mathbf{G}$, $\mathbf{A}$ and the column vectors $\mathbf{a}$, $\mathbf{c}$ are defined by

$$\mathbf{G} = \begin{pmatrix} \mathbf{G}_{11} & \mathbf{0} \\ \mathbf{0} & \mathbf{G}_{22} \end{pmatrix}, \quad \mathbf{A} = \begin{pmatrix} \mathbf{A}_{11} & \mathbf{A}_{12} \\ \mathbf{A}_{21} & \mathbf{A}_{22} \end{pmatrix}, \quad \mathbf{a} = \begin{pmatrix} \mathbf{a}_1 \\ \mathbf{a}_2 \end{pmatrix}, \quad \mathbf{c} = \begin{pmatrix} \mathbf{c}_1 \\ \mathbf{c}_2 \end{pmatrix}, \tag{41}$$

with elements $(m, n = 1, \ldots, M; k, l = 1, \ldots, L)$

$$\begin{aligned} &A_{11}(l,k) = \left(\psi_l, \mathsf{K}\frac{\psi_k}{r}\right), \quad A_{12}(l,m) = (\psi_l, \mathsf{K}\phi_m), \quad A_{21}(n,l) = \left(r\phi_n, \mathsf{K}\frac{\psi_l}{r}\right), \\ &A_{22}(n,m) = (r\phi_n, \mathsf{K}\phi_m), \qquad G_{11}(l,k) = \frac{D_l}{R^c}\delta_{kl}, \qquad G_{22}(n,m) = (r\phi_n, \phi_m), \qquad a_1(l) = \alpha_0^{(l)}, \\ &a_2(m) = \alpha_m, \qquad c_1(l) = \frac{D_l}{R^c}C_l, \qquad c_2(m) = 0. \end{aligned} \tag{42}$$

The way we solve this matrix equation is explained in Sect. 3.2. We first show how the entries of the matrices are computed.

We introduce shifted and scaled Legendre polynomials, $P_{s,q}(r; c_q; d_q)$, of order s, defined on strip $q (q = 1, \ldots, N)$ as

$$P_{s,q}(r; c_q; d_q) = P_s\left(\frac{r - c_q}{d_q}\right), \qquad r \in [r_0^{(q)}, r_1^{(q)}], \tag{43}$$

where

$$c_q = \frac{r_1^{(q)} + r_0^{(q)}}{2}, \qquad d_q = \frac{r_1^{(q)} - r_0^{(q)}}{2}, \qquad q = 1, \ldots, N, \tag{44}$$

and $P_{s,q}(r; c_q; d_q) = 0$ for $r \notin [r_0^{(q)}, r_1^{(q)}]$. Orthogonality of Legendre polynomials yields

$$\int_{S_\cup^r} \frac{P_{s,q}(\rho; c_q; d_q)}{\rho} P_{s',q'}(\rho; c_{q'}; d_{q'})\rho \, \mathrm{d}\rho = \frac{2d_q}{2s+1}\delta_{ss'}\delta_{qq'}. \tag{45}$$

The shifted and scaled Legendre polynomials are used to construct the basis functions. We create a series expansion in different basis functions for each strip separately, that is,

$$j_\perp = \sum_{s=1}^{S}\sum_{q=1}^{N} \alpha_{s,q}\phi_{s,q} + \sum_{t=1}^{N-L} \alpha_{0,t}\phi_{0,t}, \tag{46}$$

where S denotes the number of degrees of basis functions that is included.
Requirements for the basis $\phi_{s,q}$ functions is that $(\phi_{s,q}, r\phi_{s',q'}) = 0$ for $s \neq s'$ or $q \neq q'$ and $(\phi_{s,q}, \psi_l) = 0$ for all s and l. For Legendre polynomials of degree one and higher, we have

$$\int_{S_\cup^r} \frac{P_{s,q}(\rho; c_q; d_q)}{\rho} \psi_l(\rho)\rho \, \mathrm{d}\rho = 0, \tag{47}$$

for $q = 1, \ldots, N, l = 1, \ldots, L$, and $s \geq 1$. Therefore, we can choose the basis functions of degree one and higher equal to the shifted and scaled Legendre polynomials:

$$\phi_{s,q} = \frac{1}{r}P_{s,q}(r; c_q; d_q), \qquad q = 1, \ldots, N, \quad s = 1, \ldots, S. \tag{48}$$

The functions $\phi_{0,t}, t = 1, \ldots, N - L$ together with the functions $r^{-1}\psi_l, l = 1, \ldots, L$ establish an orthogonal system with the same linear span as $\{r^{-1}P_{0,q}(\rho; c_q; d_q) | q = 1, \ldots, N\}$, satisfying

$$\begin{aligned} &(\phi_{0,t}, r\phi_{0,t'}) = \delta_{tt'}, \qquad t, t' = 1, \ldots, N - L, \\ &(\phi_{0,t}, r\psi_l) = 0, \qquad t = 1, \ldots, N - L, \quad l = 1, \ldots, L; \end{aligned} \tag{49}$$

for more details see [4, Sect. 3].

It is convenient to transform all intervals $[r_0^{(q)}, r_1^{(q)}]$ to $[-1, 1]$. For the entries of $\mathbf{A}$, we have to compute integrals of the form

$$d_q d_{q'} \int_{-1}^{1}\int_{-1}^{1} P_{s'}(r)P_s(\rho)\mathcal{K}(d_{q'}r + c_{q'}, d_q\rho + c_q)(d_{q'}r + c_{q'})\,\mathrm{d}\rho\,\mathrm{d}r. \tag{50}$$

Since the integrands are logarithmically singular if $q = q'$, we extract the logarithmic part, which is obtained explicitly from the asymptotic expansion of $\mathcal{K}(r, \rho)$ for r close to ρ:

$$r\mathcal{K}(r, \rho) \approx -\frac{1}{2\pi}\left(\log|r-\rho| - \log\sqrt{r\rho} - \log 2 + \Gamma^{(0)}\left(\frac{3}{2}\right) + \gamma\right), \qquad |r-\rho| \ll 1, \tag{51}$$

where $\Gamma^{(0)}(3/2) \approx 0.03649$ ($\Gamma^{(0)}$ is the polygamma function), and $\gamma \approx 0.57722$ (Euler's constant); see [15]. The difference between $r\mathcal{K}(r, \rho)$ and this asymptotic expansion is a regular function.

In computing integrals of the type (50), we use the following explicit result:

$$\int_{-1}^{1}\int_{-1}^{1} P_k(r)P_{k'}(\rho)\log|r-\rho|\,\mathrm{d}\rho\,\mathrm{d}r = \begin{cases} \dfrac{8}{(k+k')(k+k'+2)[(k-k')^2-1]}, & \text{if } k+k' > 0 \text{ even}, \\ 0, & \text{if } k+k' \text{ odd}, \\ 4\log 2 - 6, & \text{if } k = k' = 0. \end{cases} \tag{52}$$

For the derivation of this relation, we refer to [16]. The remaining difference function is regular and can therefore be integrated numerically. We will use the Gauss–Legendre quadrature rule as integration method. We note that the singular logarithmic part of the integral kernel governs the behavior of the current distribution $j(r)$; the contributions of the regular part are small.

3.2 Solving the linear set of equations

In this section, we describe the solution procedure for Eq. (40). In this equation, the unknowns are $\alpha_m, m = 1, \ldots, M$, C_l and $\alpha_0^{(l)}, l = 1, \ldots, L$. The coefficients C_l, introduced in (25) should be related to the L prescribed values of the total currents $\hat{I}_l$ through groups $l = 1, \ldots, L$. The parameter κ has a known value and the entries of $\mathbf{G}$ and $\mathbf{A}$ can be determined from (42). Additionally, the total currents $\hat{I}_1, \ldots, \hat{I}_L$ in the L groups are given. According to (28) they yield the relations

$$\int_{S_\cup^r} j(\rho)\frac{\psi_l(\rho)}{\rho}\rho\,\mathrm{d}\rho = \alpha_0^{(l)}\left(\frac{\psi_l}{r}, \frac{\psi_l}{r}\right) + \sum_{m=1}^{M}\alpha_m\left(\phi_m, \frac{\psi_l}{r}\right) = \hat{I}_l, \qquad l = 1, \ldots, L. \tag{53}$$

We use these relations to eliminate the L unknown coefficients C_l. To this end, we define the $L \times (L + M)$ matrix $\mathbf{S}$ by

$$\mathbf{S} = \begin{pmatrix}\mathbf{S}_{11}\ \mathbf{S}_{12}\end{pmatrix}, \tag{54}$$

with elements ($m = 1, \ldots, M$; $k, l = 1, \ldots, L$)

$$S_{11}(l, k) = \left(\frac{\psi_l}{r}, \frac{\psi_k}{r}\right)\delta_{kl}, \quad S_{12}(l, m) = \left(\frac{\psi_l}{r}, \phi_m\right), \tag{55}$$

where the latter elements are only non-zero if ϕ_m acts on a ring in group l. Moreover, let $\hat{\mathbf{I}}$ be the L-vector consisting of all $\hat{I}_l, l = 1, \ldots, L$. Then, (53) can be written in matrix form:

$$\mathbf{Sa} = \hat{\mathbf{I}}. \tag{56}$$

Thus, the vector $\mathbf{a}$ of length $L+M$ is transformed into the vector $\hat{\mathbf{I}}$ of length L. The vector $\mathbf{c}$ in the right-hand side of (40) also has length $L+M$. However, only the first L entries are unknown (representing C_l); the other entries are equal to zero. To reduce also the vector $\mathbf{c}$ to a vector of length L, we introduce the $(L+M)\times L$ matrix $\mathbf{B}$ and the L-vector $\hat{\mathbf{c}}$, by

$$\mathbf{B}=\begin{pmatrix}\mathbf{B}_{11}\\ \mathbf{B}_{21}\end{pmatrix},\qquad \mathbf{c}=\mathbf{B}\hat{\mathbf{c}}, \tag{57}$$

where $(m=1,\ldots,M;\, k,l=1,\ldots,L)$

$$B_{11}(l,k)=\frac{D_l}{R^c}\delta_{kl},\qquad B_{21}(m,k)=0, \tag{58}$$

and

$$\hat{c}(l)=C_l. \tag{59}$$

We know that $(\mathbf{G}-\mathrm{i}\kappa\mathbf{A})$ is invertible, and so the matrix equation (40) reveals that $\mathbf{a}=(\mathbf{G}-\mathrm{i}\kappa\mathbf{A})^{-1}\mathbf{c}$. According to (56) and $(57)_2$, the two L-vectors $\hat{\mathbf{I}}$ and $\hat{\mathbf{c}}$ are related to each other by

$$\mathbf{S}(\mathbf{G}-\mathrm{i}\kappa\mathbf{A})^{-1}\mathbf{B}\hat{\mathbf{c}}=\hat{\mathbf{I}}, \tag{60}$$

or

$$\hat{\mathbf{c}}=[\mathbf{S}(\mathbf{G}-\mathrm{i}\kappa\mathbf{A})^{-1}\mathbf{B}]^{-1}\hat{\mathbf{I}}, \tag{61}$$

since also $\mathbf{S}(\mathbf{G}-\mathrm{i}\kappa\mathbf{A})^{-1}\mathbf{B}$ is invertible.

At this point, we have eliminated the unknown coefficients C_l in favor of the given $\hat{I}_l$, $l=1,\ldots,L$. The right-hand side of (40) becomes

$$\mathbf{c}=\mathbf{B}\hat{\mathbf{c}}=\mathbf{B}[\mathbf{S}(\mathbf{G}-\mathrm{i}\kappa\mathbf{A})^{-1}\mathbf{B}]^{-1}\hat{\mathbf{I}}=:\mathbf{C}\hat{\mathbf{I}}, \tag{62}$$

where $\mathbf{C}$ is a known $(L+M)\times L$ matrix. The fundamental unknown $(L+M)$-vector $\mathbf{a}$, containing the unknowns $\alpha_0^{(l)}$ and α_m, is governed by the matrix equation in its ultimate form

$$(\mathbf{G}-\mathrm{i}\kappa\mathbf{A})\mathbf{a}=\mathbf{C}\hat{\mathbf{I}}. \tag{63}$$

This linear set of equations will be solved numerically. The results for two different sets of circular strips will be presented in the next section.

4 Numerical results

In this section we present numerical results for the current distributions for, firstly, a set of one circular strip, and, secondly, for a set of 10 strips. We also computed the total resistance and the dissipated power of the two sets for a range of frequency values.

4.1 Single plane circular strip

We first consider one circular loop of width $D=2\,\mathrm{cm}$, thickness $h=2.5\,\mathrm{mm}$, and inner and outer radius $r_0=32.33\,\mathrm{cm}$ and $r_1=34.33\,\mathrm{cm}$, respectively. The amplitude of the total current on the loop is $I=600$ A.

In Fig. 3, the amplitude of the current distribution in the strip is shown as a function of r for the four frequencies $f=\omega/2\pi=100, 400, 700, 1,000\,\mathrm{Hz}$. For low frequencies, the current tends to the DC solution, which can be determined analytically from (16). Note that in (16) the variables j and r are dimensionless. In dimensional form we obtain

$$j(r)=\frac{I}{r\log(r_1/r_0)}=\frac{1.0}{r}\times 10^4\,\mathrm{A/m}. \tag{64}$$

The value of the average current is $j^c=I/D=3.0\times 10^4\,\mathrm{A/m}$.

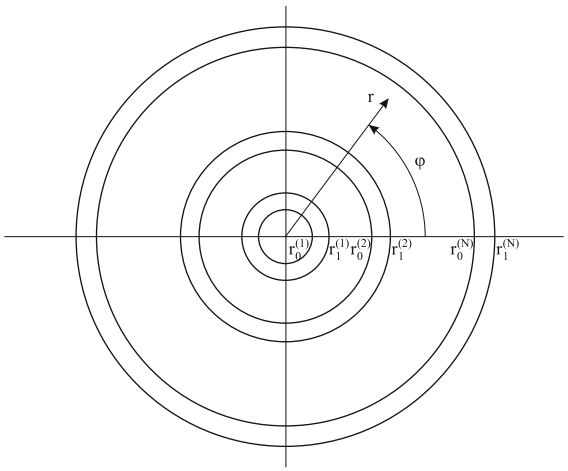

Fig. 2 The configuration of a set of plane circular strips

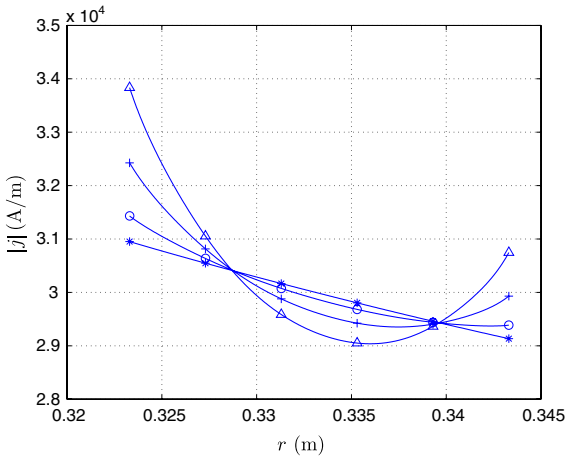

Fig. 3 Amplitude of the current distribution in one circular loop of 2 cm width with a total current of 600 A at frequencies $f = 100\,\text{Hz}$ ($*$), $f = 400\,\text{Hz}$ ($\circ$), $f = 700\,\text{Hz}$ ($+$), $f = 1{,}000\,\text{Hz}$ ($\triangle$)

On the scale used in Fig. 3, the current distribution at $f = 100\,\text{Hz}$ cannot be distinguished from the DC solution, but for higher frequencies edge-effects become visible. In contrast to the situation of a single ring, see [4], the edge-effects are not symmetric in the circular loop. The current near the inner edge of the loop has a higher value than near the outer edge; the main part of the current distribution shifts towards the inner edge of the loop. A direct consequence of this shift is that the magnetic field along the axis of symmetry of the loop, which is induced by the circular loop, increases and deviates from the desired field. Hence the designer of a transverse gradient coil has to compensate for this amplified field strength.

In comparison with the uniform current distribution that is assumed in the design approach using streamlines, two effects play a role in the distortion of the desired field. First, the current is more dense near the inner edge of the loop than near the outer edge, because of the variation of their circumferential lengths. We refer to this effect as the $1/r$-effect, and we note that it also occurs in the static DC situation. The second effect, the edge-effect, occurs only in a dynamic situation and is caused by induction.

In our approach the Petrov–Galerkin method is applied to solve the basic integral equation. Global basis functions, with unlimited support, are defined on the whole domain of the strips. The resulting matrices are of small size, but dense. Another option to solve the integral equation for the current distribution is by using local basis functions, with local support, in the Galerkin method. The matrices are then sparse, but of large size. We have performed such computations with the finite-element package `sysiphos` (in cooperation with Dr. H. De Gersem, Technische Universität Darmstadt). The field-circuit coupling that is implemented is described in [17], the solver in [18], and the necessary adaptive mesh refinement in [19]. This 2D solver computes the current distribution through a cross-section of finite thickness. In order to obtain a good approximation of the current, a very fine mesh needs to be generated. Since the thickness of the strip is very small, in this direction the elements have a size in the order of tenths of a millimeter. However, as we are mainly interested in the current distribution in the radial direction, we need a fine mesh in that direction as well. Finally, because the domain of the vector potential extends to the space outside the (cross-section of the) strip, also the vacuum space around the strip must be meshed. All this easily leads to a matrix system with millions of elements, resulting in large computing times. However, for a validation of the results of our approach involving global basis functions, it has been worthwhile to do the finite-element computations. We obtained exactly the same current distributions with the two methods.

For a second validation, we have computed the resistance of the strip. Again, both our method and the FEM method yield the same results. This is shown in Fig. 4. The electrical resistance for a three-dimensional body $\mathcal{V}$, carrying a time-harmonic current with, complex, spatial density $\mathbf{J}$ and total current I, is defined as

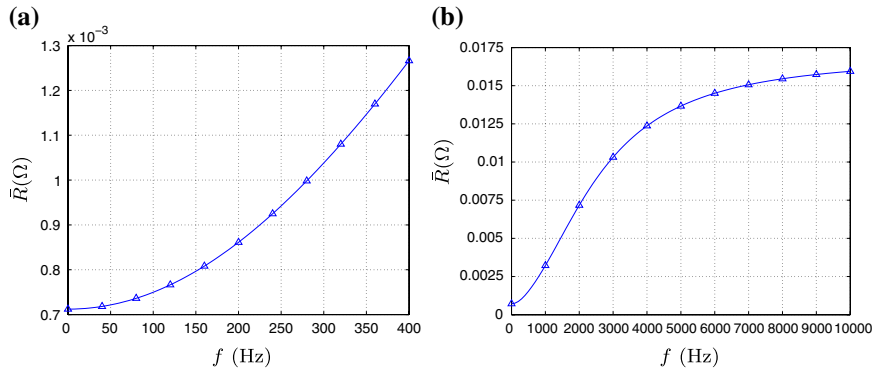

Fig. 4 A single circular strip of 2 cm width with a total current of 600 A. (**a**) Resistance $\bar{R}$ at frequencies up to $f = 400$ Hz; (**b**) Resistance $\bar{R}$ at frequencies up to $f = 10{,}000$ Hz. The symbols $\triangle$ denote the FEM results

$$\bar{R} = \frac{1}{\sigma I^2} \int_{\mathcal{V}} \mathbf{J} \cdot \mathbf{J}^* \, \mathrm{d}v, \tag{65}$$

where the asterisk denotes the complex conjugate. For the two-dimensional strip, with $\mathbf{J} \cdot \mathbf{J}^* \to (j_c/h)^2 j(r)$ and $j_c = I/D$, this formula simplifies to

$$\bar{R} = \frac{2\pi r_0^2}{h\sigma D} \int_1^{r_1/r_0} r j^2(r) \, \mathrm{d}r. \tag{66}$$

For the DC case, the resistance can be calculated analytically, yielding

$$\bar{R}_{\mathrm{DC}} = \frac{2\pi}{h\sigma \log(r_1/r_0)} = 7.12 \times 10^{-4} \Omega. \tag{67}$$

For the time-harmonic case, Fig. 4a presents values of $\bar{R}$ for the low-frequency range from 0 to 400 Hz. Figure 4b represents the higher-frequency range from 0 to 10,000 Hz, showing the behavior after the point of inflection.

4.2 Ten plane circular strips

In the practical design of x-coils and y-coils, specific software is used to compute a stream function. The stream function has a shape that is well approximated by a cosine function. Here, we define the stream function $s(r)$ as

$$s(r) = \begin{cases} I_{\max} \cos\left(\dfrac{\pi r}{2R_{ref}}\right), & \text{if } |r| < R_{\mathrm{ref}}, \\ 0, & \text{if } |r| > R_{\mathrm{ref}}, \end{cases} \tag{68}$$

where R_{ref} is the radius that defines the support domain of $s(r)$, and $I_{\max}$ represents the maximum value of $s(r)$. The stream function is discretized by means of streamlines, which form circles for fixed values of r. Each streamline forms the central line of a plane circular loop. The number of streamlines and the widths of the loops are such that the strips do not overlap.

In case we want to specify N plane circular loops with central lines at positions $r = r^{(n)}$, $n = 1, \ldots, N$, and with each loop carrying the same total current, the discretization can be made according to equidistant steps in the stream function. Then, each loop has a total current of $I^{(n)} = I_{\max}/N$, and the positions $r^{(n)}$ are determined from

$$\cos\left(\frac{\pi r^{(n)}}{2R_{\mathrm{ref}}}\right) = \frac{1}{2N}(2n-1), \qquad n = 1, \ldots, N, \tag{69}$$

such that

$$r^{(n)} = \frac{2R_{\mathrm{ref}}}{\pi} \arccos\left(\frac{2n-1}{2N}\right). \tag{70}$$

Table 1 Inner and outer radii of the set of 10 circular loops

Ring	Inner radius (cm)	Outer radius (cm)
1	9.11	11.11
2	16.66	18.66
3	22.01	24.01
4	26.48	28.48
5	30.46	32.46
6	34.14	36.14
7	37.62	39.62
8	40.96	42.96
9	44.21	46.21
10	47.41	49.41

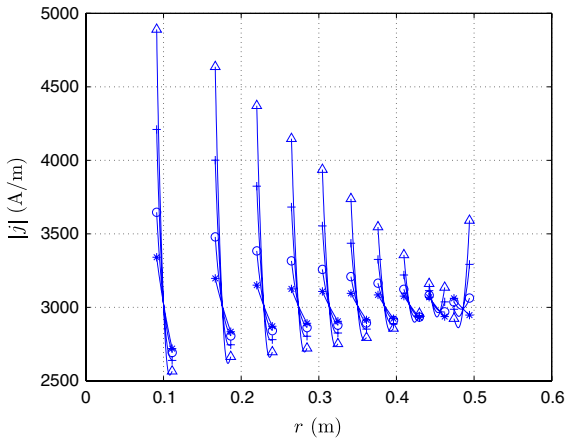

Fig. 5 Amplitude of the current distribution in a set of 10 circular loops of 2 cm width, each with a total current of 60 A, at frequencies $f = 100\,\text{Hz}$ ($*$), $f = 400\,\text{Hz}$ ($\circ$), $f = 700\,\text{Hz}$ ($+$), $f = 1,000\,\text{Hz}$ ($\triangle$)

The configuration we consider here consists of 10 circular loops, all of width 2 cm; its domain is limited by $R_{\text{ref}} = 0.5\,\text{m}$. The maximum value of the stream function is chosen as $I_{\max} = 600\,\text{A}$. The inner radii $r_0^{(n)}$ and the outer radii $r_1^{(n)}$, as found from (70), are listed in Table 1, for $n = 1, \ldots, 10$. The total current in each ring is $I^{(n)} = I_{\max}/N = 60\,\text{A}$. The applied currents have a frequency $\omega = 2\pi f$ and are in phase.

The resulting current distributions within the loops are calculated from (63). In Fig. 5, the amplitudes of the current distributions in the 10 loops are depicted for $f = 100, 400, 700, 1{,}000\,\text{Hz}$. The average current in each ring is $j^c = 3.0 \times 10^3\,\text{A/m}$. In the DC situation, the current is distributed according to the analytical formula

$$j(r) = \sum_{n=1}^{N} \frac{I^{(n)}}{\log\left(r_1^{(n)}/r_0^{(n)}\right)} \frac{\psi_n(r)}{r}, \tag{71}$$

where $\psi_n(r)$ is the characteristic function of loop n.

In Fig. 5, the current distribution at 100 Hz is very close to the DC solution, but for higher frequencies in each loop local edge-effects become visible. Moreover, when considering the envelope of the graph, a global edge-effect is observed. Analogous results were found for a set of coaxial rings in [4]. However, in contrast to [4], here both the local and the global edge-effect are not symmetric: it is in all loops and in the set as a whole more pronounced near the inner edges. This will result in an amplified magnetic field along the axis of symmetry, which should be compensated in the ultimate design.

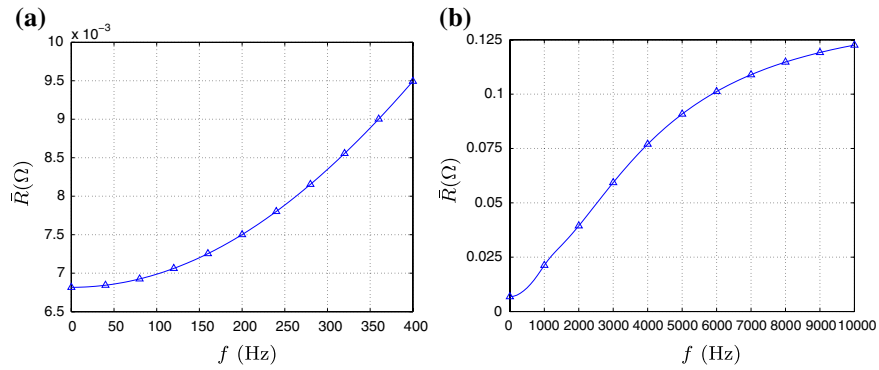

Fig. 6 Total resistance of a set of 10 circular loops of 2 cm width carrying a total current of 60 A per loop in phase. (**a**) Resistance $\bar{R}$ at frequencies up to $f = 400$ Hz; (**b**) Resistance $\bar{R}$ at frequencies up to f = 10,000 Hz. The symbols $\triangle$ denote the FEM results

We have also computed the total resistance of the set of loops by means of formula (65). In the DC situation, the current is given by (71), which yields the following value for the resistance:

$$\bar{R}_{\mathrm{DC}} = \frac{2\pi}{h\sigma} \sum_{n=1}^{10} \frac{1}{\log\left(r_1^{(n)}/r_0^{(n)}\right)} = 6.816 \times 10^{-3}\,\Omega. \tag{72}$$

For frequencies in the range from 0 to 400 Hz, the results are shown in Fig. 6a. The symbols $\triangle$ denote the FEM results. We conclude that the results of our method and those of the finite-element method coincide. Moreover, to show the behavior of the resistance after the point of inflection, in Fig. 6b, we have depicted the computed values of $\bar{R}$ for the range from 0 to 10,000 Hz as well.

The dissipated power in a set of loops is defined as

$$P_{\mathrm{diss}} = I^2 \bar{R}. \tag{73}$$

As an example, we calculate the dissipated power for the two sets considered here at a frequency $f = 1,000$ Hz. For the first set of one strip, with a current $I = 600$ A and a resistance $\bar{R} = 3.2 \times 10^{-3}\Omega$, we find $P_{\mathrm{diss}} = 1.15 \times 10^3$ W, whereas for the set of 10 strips, with $I = 60$ A and $\bar{R} = 2.1 \times 10^{-2}\,\Omega$, we find $P_{\mathrm{diss}} = 75.6$ W. Hence, the total dissipated power in a set of 10 strips is less than that in a set of one strip, while in both situations the same magnetic field is created in a specific region of interest (according to (68)). The overall advantage is that the current that has to be supplied to the 10 strips is 10 times less than that needed in the set of one strip.

5 Conclusions

In this paper, we have modeled a transverse (x-coil or y-coil) gradient coil by a set of curved circular loops, i.e., thin copper strips, placed on the surface of a cylinder. We have shown that locally replacing the curved surface by the tangent plane has a negligibly small effect on the current distribution in the loops. The reason is that the currents affect each other only locally. Therefore, for the current distribution in the curved circular loops on the cylindrical surface, we may use the distribution calculated for a plane circular strip model. However, this model may not be applied for the calculation of the induced magnetic field. For the latter, one must return to the original curved configuration and then by means of the Biot–Savart law the magnetic field can be calculated.

In a set of plane circular loops, the current flows in the tangential direction and depends on the radial coordinate only. The current distribution in the loops is induced by a source current. In circular loops, this source current features a $1/r$-decay in the radial direction. For this reason, we apply the Petrov–Galerkin method, in which Legendre polynomials divided by the radial coordinate are chosen as basis functions, and the Legendre polynomials themselves as test functions. For the resulting current distribution an integral equation is derived. The kernel of this integral

equation is logarithmically singular. To tackle the logarithmic part of the kernel, we use the analytical formula (52); the remaining part of the kernel is regular and computed numerically. In this way, the integral equation is reduced to a finite set of linear algebraic equations for the unknown coefficients of the basis functions. Solving this system, we obtain the current distribution we are looking for.

The resulting current distribution in the loops shows two effects that influence the induced magnetic field:

1. A decay in the current density in the radial direction, called the $1/r$-effect, a typical static effect.
2. Edge-effects, caused by eddy currents, a typical dynamic effect.

The edge-effects are more pronounced near the inner edge of the circular strip. Thus, in total, the currents are shifted towards the center of the coil. This is in contrast with the original design based on streamlines in which a uniform distribution of the current in the loops was assumed. Consequently, the induced magnetic field along the axis of symmetry of the loops is amplified, an effect that should be compensated for in the final design.

Based on the analysis in this paper we conclude that the dominant logarithmic behavior of the kernel of the governing integral equation justifies the approximation of a curved circular loop locally by a plane circular loop. The Petrov–Galerkin method, in combination with the use of Legendre polynomials, delivers us a very fast algorithm to calculate the current distribution, for which only a very small number (5–10) of basis functions are needed. We have validated our results by comparison with those of a (much more time-consuming) finite-element program, and complete correspondence was found. We observe a striking difference between a set of coaxial rings (modeling a z-coil) and one of circular loops (modeling an x-or y-coil) in so far that the latter shows a non-symmetric edge-effect (leading to the shift in the current distribution mentioned above). From Figs. 3 and 5, we conclude that this edge-effect becomes more apparent both with increasing frequency and curvature of the loops. Figure. 5 shows not only a local edge-effect per loop, but also a global one for the set as a whole. Also the magnitude of the latter effect increases with the frequency.

Finally, the total resistances of the two sets we considered were calculated (for this, not more than six coefficients were needed). As can be expected, the resistance increases with frequency. More important is the conclusion, which was also reached in [4], that the dissipated power for a set of 10 loops was less than that for a single loop, provided that both sets create the same magnetic field in a specific region of interest. Moreover, we noticed from Figs. 4 and 6 that the resistance as a function of the frequency has an inflection point. As explained in [4], this point represents the frequency at which prevailing resistive effects with respect to inductive effects change into prevailing inductive effects.

The mathematical analysis presented so far for plane rectangular strips [3], circular loops of strips [4] and transverse curved circular strips can be used for a large number of design concepts to investigate the qualitative effects of model parameters on the magnetic field. The standard shape missing in this list is the rectangular patch that is placed as an island between other conducting strips on a cylindrical surface. Research has already been conducted on these geometries ([16,Ch. 5]) and the results will be published in the near future. Due to the local induction effects, the standard shapes can be used for any arbitrary shape of conductors on a cylindrical surface.

References

1. Jin JM (1999) Electromagnetic analysis and design in magnetic resonance imaging. CRC Press, London
2. Vlaardingerbroek MT, den Boer JA (1999) Magnetic resonance imaging. Springer-Verlag, Berlin
3. Ulicevic T, Kroot JMB, van Eijndhoven SJL, van de Ven AAF (2005) Current distribution in a parallel set of conducting strips. J Eng Math 51:381–400
4. Kroot JMB, van Eijndhoven SJL, van de Ven AAF (2007) Eddy currents in a gradient coil, modeled as circular loops of strips. J Eng Math 57:333–350
5. Romeo F, Hoult DI (1984) Magnetic field profiling: analysis and correcting coil design. Magn Reson Med 1: 44–65
6. Suits H, Wilken DE (1989) Improving magnetic field gradient coils for nmr imaging. J Phy E: Instrum 22:565–573

7. Wong E, Jesmanowicz A (1991) Coil optimization for mri by conjugate gradient descent. Magn Reson Med 21:39–48
8. Crozier S, Doddrell DM (1993) Gradient coil design by simulated annealing. J Magn Reson 103:354–357
9. Frenkiel TA, Jasinski A, Morris PG (1988) Apparatus for generation of magnetic field gradient wave forms. J Phys E: Sci Instrum 21:374–377
10. Siebold H (1990) Gradient field coils for mr imaging with high spectral purity. IEEE Trans Magn 26:897–900
11. Peeren GN (2003) Stream function approach for determining optimal surface currents. PhD thesis, Eindhoven University of Technology
12. Peeren GN (2003) Stream function approach for determining optimal surface currents. J Comput Phys 191:305–321
13. Turner R (1986) A target field approach for optimal coil design. J Phys D: Appl Phys 19:147–151
14. Tomasi D (2001) Stream function optimization for gradient coil design. Magn Reson Med 45:505–512
15. Abramowitz M, Stegun IA (1968) Handbook of mathematical functions with formulas, graphs and mathematical tables. Dover Publications, New York
16. Kroot JMB (2005) Analysis of eddy currents in a gradient coil. PhD thesis, Eindhoven University of Technology
17. De Gersem H, Mertens R, Pahner U, Belmans R, Hameyer K (1998) A topological method used for field-circuit coupling. IEEE Trans Magn 34:3190–3193
18. De Gersem H, Lahaye D, Vandewalle S, Hameyer K (1999) Comparison of quasi minimal residual and bi-conjugate gradient iterative methods to solve complex symmetric systems arising from time-harmonic magnetic simulations. COMPEL 18:298–310
19. Mertens R, Pahner U, De Gersem H, Belmans R, Hameyer K (1998) Improving the overall solver speed: a fast, reliable and simple adaptive mesh refinement scheme. In: The 4th international workshop on electric and magnetic fields, Marseille, France, May 12–15, pp 385–390